

## Article

# A Versatile Aerial Manipulator Design and Realization of UAV Take-Off from a Rocking Unstable Surface

Hannibal Paul , Ryo Miyazaki , Takamasa Kominami , Robert Ladig  and Kazuhiro Shimonomura 

Department of Robotics, Ritsumeikan University, Kyoto 525-8577, Japan;

rr0045vp@ed.ritsumei.ac.jp (R.M.); rr0068vp@ed.ritsumei.ac.jp (T.K.); ladig@fc.ritsumei.ac.jp (R.L.)

\* Correspondence: 21v00271@gst.ritsumei.ac.jp (H.P.); skazu@fc.ritsumei.ac.jp (K.S.)

**Abstract:** UAVs are one of the fastest types of robots that can be deployed in a remote environment. Unfortunately, they have a limited flight time and therefore may need to stop occasionally in an unknown, uncontrolled area. However, conventional UAVs require flat and stationary surfaces for a safe landing and take-off. Some studies on adaptive landing approach for UAVs can be found in the past, but adaptive take-off from non-flat surfaces has not been discussed for the most part, yet. In this work, we discuss the problems associated with a conventional UAV take-off from non-flat surfaces and provide a novel approach for UAV take-off from a sloped or rocking surface. We also discuss the design of a novel multitasking three-arm aerial manipulator system with parallel link mechanism and achieve the above-mentioned task. With experiments, we show that the system can provide stability for a UAV landing on a rocking surface that allows for a safe take-off.

**Keywords:** aerial manipulator; adaptive landing; adaptive take-off; aerial robotics; multitasking UAV



**Citation:** Paul, H.; Miyazaki, R.; Kominami, T.; Ladig, R.; Shimonomura, K. A Versatile Aerial Manipulator Design and Realization of UAV Take-Off from a Rocking Unstable Surface. *Appl. Sci.* **2021**, *11*, 9157. <https://doi.org/10.3390/app11199157>

Academic Editor: Wojciech Giernacki

Received: 2 September 2021

Accepted: 27 September 2021

Published: 1 October 2021

**Publisher's Note:** MDPI stays neutral with regard to jurisdictional claims in published maps and institutional affiliations.



**Copyright:** © 2021 by the authors. Licensee MDPI, Basel, Switzerland. This article is an open access article distributed under the terms and conditions of the Creative Commons Attribution (CC BY) license (<https://creativecommons.org/licenses/by/4.0/>).

## 1. Introduction

UAVs are a very suitable candidate when it comes to search-and-rescue operations using robots. Their capability to hover and maneuver in the skies allows them to receive ground information from high vantage points. This is shown in studies such as [1,2], concentrating on employing UAVs to map the terrain using camera images after a disaster. UAVs can not only fly and collect photographs, but they can also execute aerial manipulation, given the proper on-board equipment. Research like [3] have presented a framework for valve turning employing a UAV equipped with twin manipulators. Similarly, Ref. [4] focuses on producing large force and moment exertion while employing a UAV to clear obstructions using manipulation by pushing.

However, a UAV's payload always limits its potential flying time. Because there is a limit on the size and weight of batteries that can be carried, effective flight management is required as well. Docking or landing a UAV is a preferable option rather than continually hovering in mid-air to extend the work time when the UAV is idle while deploying it across long distances. The work in [5] provides a mechanism to perch a UAV on a farm post using a manipulator mounted on the bottom part of the UAV. However, the work in [6] proposes a bio-inspired multi-modal UAV that flies, perches, and climbs on external surfaces such as concrete or stucco walls. Our previous work in [7], describes the development of a gripper mounted on the top part of a UAV to dock the UAV on pipes. Furthermore, similar to the water sampling in [8], other data collection activities, such as soil samples, may be conducted while the UAV is landed on a surface.

Many previous studies have concentrated on developing an autonomous landing system for UAVs that would be suited for carrying out the aforementioned tasks. Manually landing a UAV in an unfamiliar location is a time-consuming and difficult process due to environmental clutter. Furthermore, manually landing through remote tele-operation necessitates the use of a qualified operator. Studies such as [9,10], focus on autonomously landing a UAV using camera information. A DARPA funded research in [11] developed

adaptable landing gears for a helicopter to quickly and safely land on an irregular surface. In prior work, we designed a UAV with a three-arm aerial manipulator system (TAMS) [12] to execute a variety of tasks, including vision-based adaptive landing, which can be very useful in disaster events.

A VTOL UAV requires less room for landing (theoretically, only the diameter of its airframe plus the propeller span). When considering a traditional VTOL-type UAV, however, it is always required to ensure that the airframe is aligned with the horizon. Failure to fulfill this requirement will often result in unexpected UAV movements and a crash. To minimize unexpected movements, some current off-the-shelf flight controllers will not let the propellers start spinning if the airframe is not parallel to the horizon. Previously, in [13], we accomplished adaptive landing with a UAV employing three manipulators to safely land on uneven surfaces and avoid rolling accidents. However, unlike a stable surface, the landed surface may alter after landing due to disturbances. A rocking ship deck is one of the excellent examples for an unstable surface targeted by this approach. An adaptive landing system could aid in landing and would operate until the UAV lands on a moving ship deck; but because the ship deck is not stable, the UAV would not be able to take off safely from this surface. As a result, the UAV would not be able to return to its base station, resulting in a failed mission. A mechanism for airframe stabilization is necessary to keep the airframe parallel to the horizon at all times, even after landing, for safe take-off in this scenario.

This work focuses on two fundamental ideas. The first consideration is the manipulator's design. We suggest a novel manipulator system with a lesser number of actuation when compared to other research using general-purpose manipulator systems [3,14] for a particular task. This is especially important in the case of aerial manipulation to decrease power consumption because the battery size is restricted by payload constraints. The second step is to demonstrate the stability of the UAV's airframe after landing by employing manipulators against changing ground elevation as seen in Figure 1. We show that with our system, a UAV can land and take-off on uneven ground even if the ground slope varies.

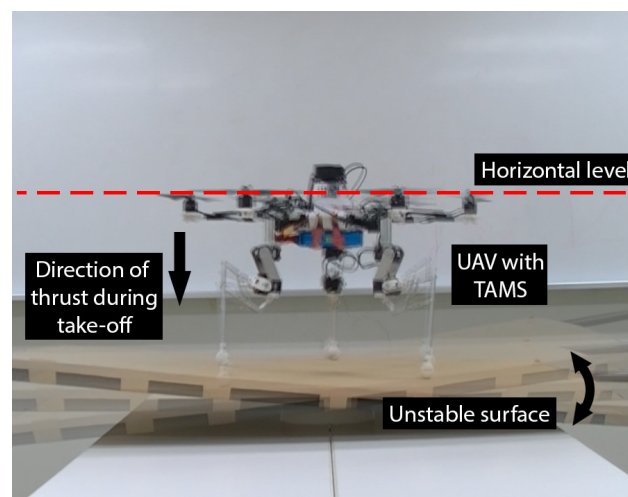


**Figure 1.** The UAV with three-arm aerial manipulator system landed and ready to take off from an unstable platform with changing slope.

In Section 2, the concept and design requirements for a manipulator system is discussed with the objective to attain various heterogeneous aerial manipulator tasks using TAMS. Section 3 provides the hardware description of the manipulator system, kinematics and the airframe size required to extend the workspace of the manipulators. The control system for the airframe stabilization against surface slope variation is explained in Section 4. The experiments conducted and the results obtained are shown in Section 5, for the airframe stability task. In Section 6, discussion about the experimental results and scope for future development is provided, followed by a conclusion in Section 7.

## 2. Versatile Task Manipulator System Design

When it comes to deploying robots in the field, one of the most crucial factors to consider is multitasking. When a robot is deployed in a remote location to complete a mission, it may encounter some unexpected circumstances. Failure to address such a circumstance may result in the failure of the mission. As a result, a field robot must be able to execute a variety of roles. Some examples of recent literature focusing on the development of versatile robots can be found in [15–17]. Ross Robotics [18], a start-up company, are producing modular, adaptive, and cost-effective unmanned ground vehicles (UGVs) that can readily adapt to do any variety of activities in hazardous situations, to substitute humans in regions where human labor is too risky. UAVs have been long used to perform a wide range of individual tasks such as surveillance [19], package delivery [20], search and rescue [21], communication assistance [22] and so on, but there are very few approaches on using a UAV to perform heterogeneous tasks. A rare example would be the work in [23], providing a collaborative planning of multitask missions using a fleet of UAVs fitted with a standard set of accessories that enable heterogeneous tasks.

A manifold of equipment must be put on-board a UAV to perform diverse tasks. However, as mentioned above, a UAV has very restricted payload and on-board power capabilities. As a result, in the development of TAMS [12], we employed three manipulators on a UAV to perform diverse tasks such as grabbing, landing and obstacle avoidance. Each of these manipulators were similar to a general-purpose four-DOF (roll, pitch, pitch and gripper) manipulator. The following points were drawn from the design of this manipulator and the tasks that we considered:

- 1 When designing the hardware for an adaptive landing system, the last link's tip must remain perpendicular to the ground to orient the link parallel to the gravity vector, reducing the stress on its joint significantly. Therefore, only its height need be changed according to the terrain and requires a minimum of 2 DOF to maintain a perpendicular posture.
- 2 When three manipulators are used to grab objects, the manipulators are regarded as a massive gripper. As a result, the angle of the link near the tip may be set, and only the link near the UAV's base is operated to open and shut the massive gripper-like structure. To open and close this massive gripper structure, at least 1 DOF is required.
- 3 When executing obstacle avoidance sideways of a UAV, the manipulators are extended or retracted while moving around the airframe, similar to the description in the adaptive landing condition (first case). Therefore, including yaw motion, to achieve this task, a minimum of 3 DOF is necessary.

A conclusion can be derived from the preceding points: Instead of employing a general-purpose manipulator design, a custom design can be used to do the same set of functions with less actuation. This is demonstrated in Figure 2, where a parallel link manipulator is shown to efficiently complete the identical set of tasks. It is sufficient to activate only one joint in each arm, by fixing the position of the other joints. As a result, motor power consumption is comparatively low. In this work we develop a new manipulator as an upgrade to our previous manipulator system in [12]. Furthermore, we show the manipulator system to carry out the additional task of horizontally stabilizing the UAV on the ground.

Type	Structure	Landing	Grasping	Obstacle avoidance
General purpose manipulator				
Parallel link manipulator				

**Figure 2.** General-purpose manipulator and parallel link manipulator design comparison for different tasks.

### 3. Hardware System Design

Multicopter aerial vehicles can outperform fixed-wing UAVs in terms of hovering capabilities and their ability to move slowly in air. This feature makes them very useful in applications from aerial photography [24] to aerial manipulation [25]. The quadrotor, with its relatively simple mechanical structure, is the most proven and widely used UAV among them, especially the commercial ones sold for recreational purposes. Another popular type of multicopter is a hexarotor [26] with six rotors mounted on an airframe. Its propulsion system provides the hexarotor with increased robustness over the quadrotor, allowing it to improve its actuator fault detection and isolation capabilities [27]. When a malfunction is detected immediately, the control law can be adjusted to meet the closed-loop criteria or to statically hover [28] or safely return the aerial vehicle to the ground if continued flight is no longer possible [29].

Usually performing aerial manipulation requires the UAV to carry additional hardware or manipulators on-board. Therefore, to safely carry this additional hardware on-board, several studies on aerial manipulation such as in [30–33] use hexarotor as their aerial platform for its higher thrust and stability. The manipulators can be mounted on different region of the airframe depending on the task. Therefore, the literature in [34] classifies various manipulator system mounted on the UAV based on the configuration of the workspace and function. In addition, the evolution and current trends in aerial robotic manipulation can be analyzed by the work in [35]. Previously, with TAMS [12], we considered the workspace such that the manipulator tips can reach the regions around, below and above the airframe. This is achieved by passing the three manipulators through the gaps in between the arms of the airframe, which are mounting the motors and rotors.

In this study, light-weight manipulators are designed and constructed using a parallel link mechanism as shown in Figure 3. The links of the arms are made of thin aluminum pipes of 10 [mm] radius. 3D-printed PLA parts are used to attach the links together with the actuator motors. For the actuation of the joints, Dynamixel AX12-A and MX-28AT motors are used.

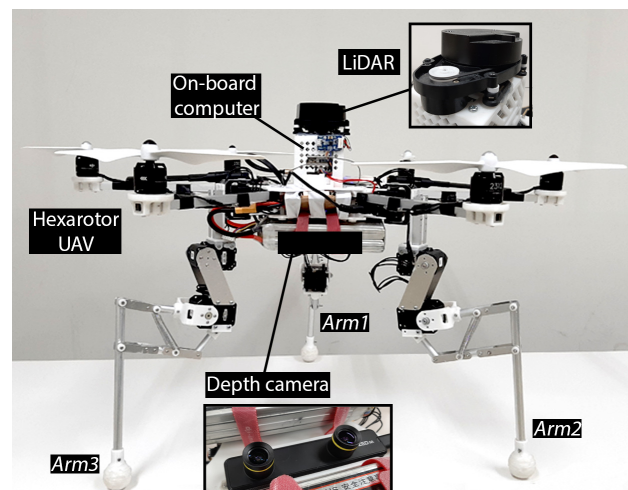


**Figure 3.** UAV with parallel link three-manipulator system.

Especially noteworthy is that for each task only one of the joints needs to be actuated (Figure 2). Additionally, when landing, the weight of the robot is strategically distributed on the manipulator's structure, without putting too much strain on the joint actuators. Although the motors could generate enough torque to hold the weight of the UAV easily, when moving the manipulator after being landed, a torque ceiling might be reached, were there not a strategic weight distribution. To assure proper torque and ability to move the frame even in extreme landing situations, a motor with higher torque (MX-28AT) is used for the last link. In addition, two extension springs are attached on each manipulator to provide some force to easily stretch the manipulator outwards. For simplicity of the design, active grippers are not attached as end-effectors. Various parameters of the developed hardware system are listed in Table 1.

**Table 1.** Parameters of the whole robot and three-arm aerial manipulator system with parallel link mechanism.

	Parameter	Value
Whole robot	Width	640 [mm]
	Maximum height	540 [mm]
	Total weight	3000 [g]
	Rotors	6
Single manipulator	DOF	3
	Link lengths (L1, L2, L3, L4, L5)	50 [mm], 40 [mm], 100 [mm], 95 [mm], 205 [mm]
	Joint angle range (J1, J2, J3)	$-100[^\circ]$ to $100[^\circ]$ , $-190[^\circ]$ to $90[^\circ]$ , $-60[^\circ]$ to $60[^\circ]$
	Maximum width	5 [mm]
	Weight	330 [g]

The kinematics of this manipulator are calculated using Equation (1), where  $s_i$  and  $c_i$  are  $\sin \theta_i$  and  $\cos \theta_i$  for  $i$ th joint respectively and  $L_1$  to  $L_5$  are the link lengths as marked in Figure 4.

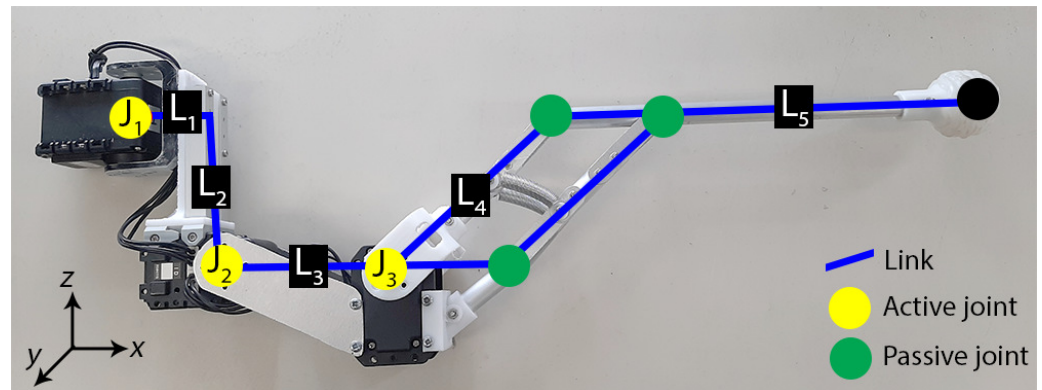


Figure 4. Link lengths and joints marked for the designed manipulator.

$$x = L_1 c_1 + L_3 c_1 c_2 - L_4 s_2 c_1 c_3 - L_4 s_3 c_1 c_2 - L_5 (s_2 s_3 c_1 - c_1 c_2 c_3) c_3 - L_5 (-s_2 c_1 c_3 - s_3 c_1 c_2) s_3, \quad (1)$$

$$y = L_1 s_1 + L_3 s_1 c_2 - L_4 s_1 s_2 c_3 - L_4 s_1 s_3 c_2 - L_5 (s_1 s_2 s_3 - s_1 c_2 c_3) c_3 - L_5 (-s_1 s_2 c_3 - s_1 s_3 c_2) s_3, \quad (2)$$

$$z = -L_2 + L_3 s_2 - L_4 s_2 s_3 + L_4 c_2 c_3 - L_5 (-s_2 s_3 + c_2 c_3) s_3 - L_5 (-s_2 c_3 - s_3 c_2) c_3 \quad (3)$$

The inverse kinematics are derived from above equations using Jacobian and are written as:

$$J_v = \begin{bmatrix} \delta_1 & \delta_2 & \delta_3 \\ \delta_4 & \delta_5 & \delta_6 \\ \delta_7 & \delta_8 & \delta_9 \\ 0 & 0 & 1 \\ 1 & 0 & 0 \\ 1 & 0 & 0 \end{bmatrix} \quad (4)$$

where

$$\begin{aligned} \delta_1 &= (-L_1 - L_3 c_2 + L_4 s_2 s_3 - L_5 c_2) s_1, \\ \delta_2 &= (L_1 + L_3 c_2 - L_4 s_2 s_3 + L_5 c_2) c_1, \\ \delta_3 &= 0, \\ \delta_4 &= -(L_3 s_2 + L_4 c_2 s_3 + L_5 s_2) c_1, \\ \delta_5 &= -(L_3 s_2 + L_4 c_2 s_3 + L_5 s_2) s_1, \\ \delta_6 &= L_3 c_2 - L_4 s_2 s_3 + L_5 c_2, \\ \delta_7 &= -L_4 c_1 c_2 s_3, \\ \delta_8 &= -L_4 s_1 c_2 s_3, \\ \delta_9 &= -L_4 s_2 s_3 \end{aligned} \quad (5)$$

The springs attached at the link  $L_4$  of the manipulator applies some torque on the Joint  $J_3$ . In other words, when the motor attached at the joint  $J_3$  does not apply any torque at this joint, the torque produced by the springs will bring the links  $L_3$  and  $L_5$  closer to each other, resulting in an extending of the manipulator. The springs are attached to link  $L_4$  as depicted in Figure 5 (marked in green). The increase in joint angle at the joint  $J_3$  will result in stretching of the spring, which in turn will induce counter torque at joint  $J_3$ . The relation between the joint  $J_3$  and spring length  $l_s$  is used to understand the spring stretching. In

Figure 5a, the set of joints marked in blue and in black are always parallel to each other. The blue dotted line is drawn parallel to the blue links from the spring intersection point at link  $P_2$ . The spring is attached between links marked as  $P_1$  and  $P_2$ . Using the triangle formed by the green, red and blue dotted lines is used to find the length  $l_s$  of the spring.

$$L_s = \sqrt{L_p^2 + L_2^2 - 2L_1L_2 \cos \theta_3} \quad (6)$$

The Equation (6) produces a relationship between the angle of the joint  $J_3$  and spring length  $l_s$ , which is shown in the form of a graph in Figure 5b.

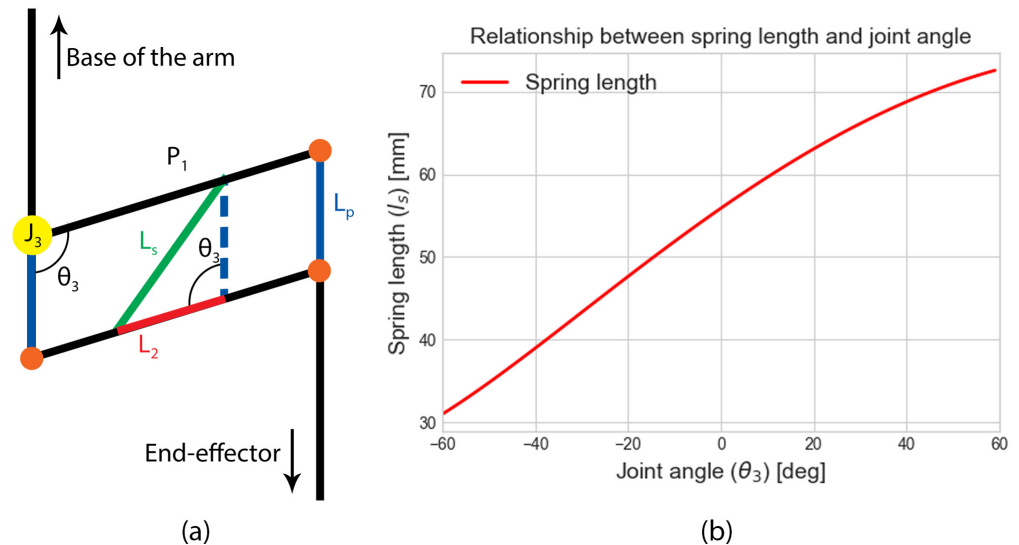


**Figure 5.** (a) Diagram to understand the spring length change in relation to joint angle; (b) relationship between spring length and joint angle  $\theta_3$ .

A hexarotor airframe is constructed using the above-described design, where the manipulators can reach below, sideways and above the airframe. Since most of the tasks such as landing and grasping requires the manipulators to be at the bottom part of the airframe, the base of the manipulators is attached at the side of the airframe, facing downwards. Although the manipulators can easily reach to the sides of the airframe from this position, to reach above it must pass between two arms of the airframe including the propeller span. Therefore, sufficient space between the propellers is required for manipulator movements in between the airframe's arms. Since the servo motors are attached directly at the joints of the manipulator links, the width of the manipulator will be equal to or more than the width of a motor. Taking into account the width of a motor and some space at either side, for a collision free up-down movement of the manipulator, at least 50 [mm] horizontal space will be needed.

According to the diagram in Figure 6, if the gap between the propellers is  $d_{gap}$ , diameter of airframe  $d_{uav}$  and the diameter of a spinning propeller is  $d_{propeller}$ , so the relationship between the three is:

$$d_{uav} = 2(d_{propeller} + d_{gap}) \quad (7)$$

The length of the propeller is predetermined as they are bought off-the-shelf. Therefore, the diameter of the UAV can be changed to satisfy our requirement. The propeller length used during this study is 240 [mm]. Therefore, using Equation (7) the airframe diameter required to pass a gripper within 50 [mm] width freely between the airframe arms will be 580 [mm]. The total weight of the UAV system along with manipulators and batteries is 3 [kg].

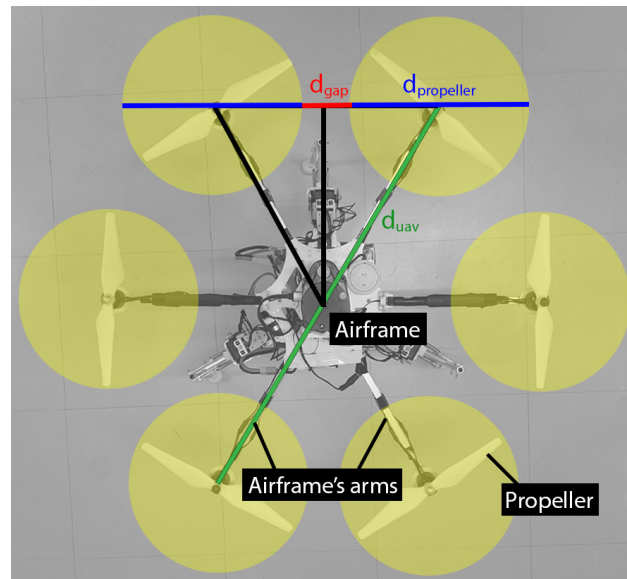


**Figure 6.** Relationship between airframe diameter, propeller length and distance between the propellers to pass the manipulators through.

#### 4. Control

Manipulator control is achieved using a Nvidia Jetson TX2, used as an on-board processor. It is also used to connect with the depth camera mounted in the bottom part of the UAV, used for grasping and landing in our previous work [12]. In this work, the IMU data acquisition and airframe leveling by controlling appropriate manipulator posture is performed in the on-board processor.

##### 4.1. Angle Change

When a surface slope changes, the elevations under a conventional UAV landing gear changes, which will in turn change the slope of the airframe. This can also occur when the UAV's legs land in between multiple surfaces and the surfaces height or slope changes randomly. When the UAV slope changes, it may lead to a rolling accident.

A rolling accident, as mentioned in [13], can occur when the projection of the center of mass of the airframe on the surface moves out of the stability polygon formed at the ground contact points. This can happen if the angle of the airframe exceeds a certain angle. The angle can be determined with the help of a diagram in Figure 7 and the following equations:

$$\begin{aligned}
 l_r &= l_a \sin 60 \\
 &= \frac{\sqrt{3}}{2} l_a \\
 l_p &= l_a \cos 60 \\
 &= \frac{l_a}{2}
 \end{aligned} \tag{8}$$

where  $l_a$  is the manipulator base mount distance from the center of the UAV,  $l_r$  is the horizontal distance from the center of the UAV to the manipulator tip  $A_2$  or  $A_3$  as seen from top view, and  $l_p$  is the vertical distance from the center of the UAV to the manipulator tips  $A_2$  and  $A_3$  when seen from top view, as shown in Figure 7.

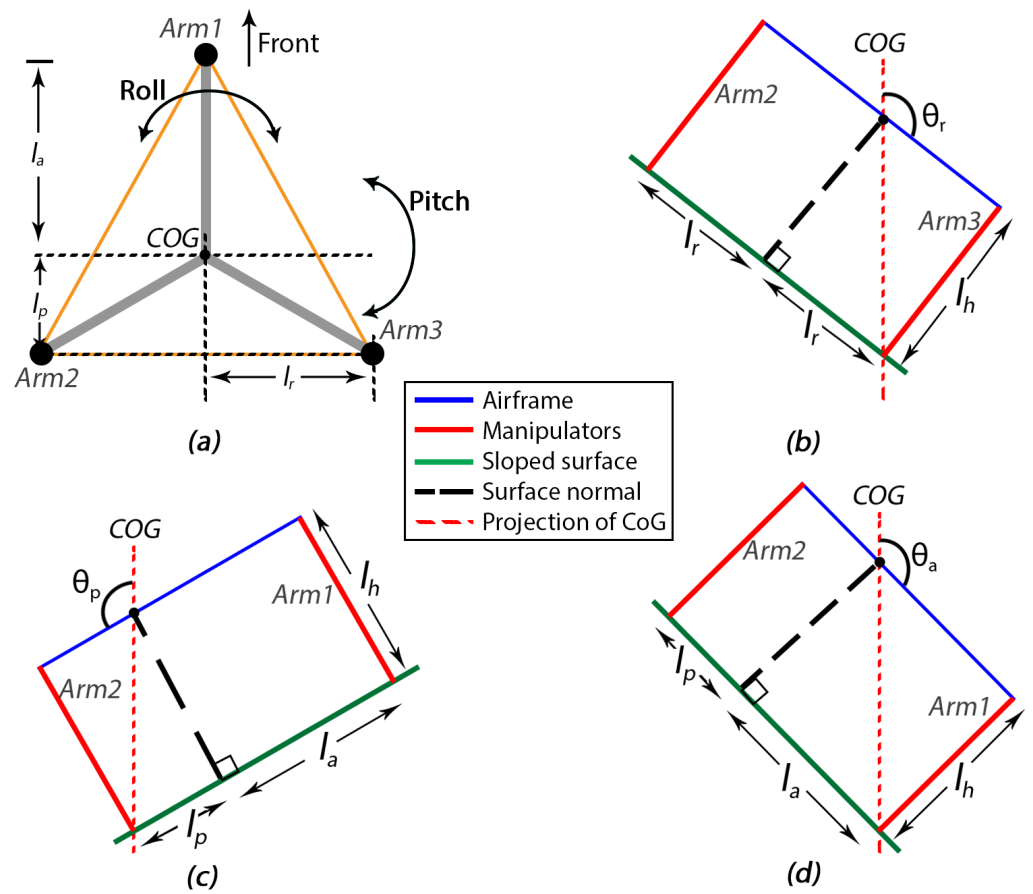


**Figure 7.** Maximum angles in roll and pitch axes of the airframe before it loses ground stability. (a) Roll and pitch axes of the UAV, its support polygon and manipulator labels. (b) Side view of COG reaching the boundary for the roll angle. (c,d) Side view of COG reaching the boundary for the pitch angles, when Arm2 (c) or Arm1 (d) side of the UAV is pointing down.

The UAV becomes unstable and will roll over if its projection of center of gravity (COG) goes out of the support polygon formed by the manipulator tips. To determine the maximum possible roll and pitch angles, the COG will be at the border of the polygon. Keeping this in mind, as depicted in Figure 7, for pitch and roll case, the angles formed this way are calculated as:

$$\begin{aligned}
 \theta_a &= 180 - \sin^{-1}\left(\frac{l_h}{\sqrt{l_a^2 + l_h^2}}\right) \\
 \theta_p &= 180 - \sin^{-1}\left(\frac{l_h}{\sqrt{l_p^2 + l_h^2}}\right) \\
 \theta_r &= 180 - \sin^{-1}\left(\frac{l_h}{\sqrt{l_r^2 + l_h^2}}\right)
 \end{aligned}
 \tag{9}$$

where \$l\_h\$ is the height of the manipulator and is variable, \$\theta\_r\$ is the roll angle of the airframe. \$\theta\_a\$ and \$\theta\_p\$ are the pitch angles of the airframe from its center to the manipulator tips \$A\_1\$ and \$A\_2 - A\_3\$ respectively. As seen in Figure 7, the relationship between \$l\_a, l\_r, l\_p\$ is:

$$l_a > l_r > l_p \tag{10}$$

Therefore, we can write the angle relations as:

$$\theta_a > \theta_r > \theta_p \tag{11}$$

In this study, the manipulator base mount distance from the center of the airframe  $l_a$  is 110 [mm]. Therefore,  $l_r$  and  $l_p$  will be 95.37 [mm] and 55 [mm] respectively from Equation (8). For the arm design in this design, the  $l_h$  is set between 282 [mm] to 417 [mm]. When it comes to the smallest  $l_h$  value (282 [mm]), using Equation (9), the maximum roll and pitch angles  $\theta_a$ ,  $\theta_p$ ,  $\theta_r$  exceeding the angle in which the UAV will roll over is 111.31[°], 101.04[°], 108.69[°] respectively. Similarly, for  $l_h$  value of 417 [mm], the maximum roll over angles  $\theta_a$ ,  $\theta_p$  and  $\theta_r$  are 104.78[°], 97.51[°] and 102.88[°] respectively.

#### 4.2. Adapting to a Surface after Landing

To adapt a landed UAV to a changing surface on which it is standing, it is necessary to know the attitude of the UAV, especially in its roll and pitch axis. Since multirotor UAVs' flight controllers are already equipped with an IMU, information about the UAV's attitude can be read from here. A controller is developed to tilt the UAV back to its zero position using the IMU data and manipulator kinematics to increase or decrease the manipulator heights accordingly. A simple PD system is developed as given in Equation (12).

$$u(t) = K_p e(t) + K_d \frac{de(t)}{dt} \quad (12)$$

where  $K_p$  and  $K_d$  are the P and D gains, respectively.  $e(t)$  is the error between the desired value and the present value.

For a stable parallel pose of the airframe, its  $\theta$  (roll angle) and  $\phi$  (pitch angle) values should be maintained zero. Therefore, any non-zero roll and pitch values forms the error  $e(t)$ . Taking into account the roll ( $\theta$ ) and pitch ( $\phi$ ) axes of the UAV and the manipulator numbering with reference to Figure 7a, Equation (12) is re-written as in Equations (13) and (14) for  $\theta$  and  $\phi$  changes respectively.

$$\begin{aligned} arm2_u(t) &= -K_p \theta(t) + K_d \dot{\theta}(t) \\ arm3_u(t) &= K_p \theta(t) + K_d \dot{\theta}(t) \end{aligned} \quad (13)$$

$$\begin{aligned} arm1_u(t) &= -K_p \phi(t) + K_d \dot{\phi}(t) \\ arm2_u(t) = arm3_u(t) &= K_p \phi(t) + K_d \dot{\phi}(t) \end{aligned} \quad (14)$$

where  $\theta(t)$  and  $\phi(t)$  are the roll and pitch values of the UAV at a given time  $t$ .  $\dot{\theta}(t)$  and  $\dot{\phi}(t)$  are the differences between the current and previous roll and pitch values respectively of the UAV.  $arm1_u(t)$ ,  $arm2_u(t)$  and  $arm3_u(t)$  are the angle changes applied to the last link of each manipulator resulting in their height changes.

The maximum slope angle of the surface till which the manipulator system will be able to maintain the airframe horizontal is:

$$\theta_{max} = \tan^{-1} \left( \frac{l_{hmax} - l_{hmin}}{d_{sep}} \right) \quad (15)$$

where  $l_{hmin}$  and  $l_{hmax}$  are the minimum and maximum controllable heights of a manipulator, which are 282 [mm] and 417 [mm] respectively in the current hardware design.  $d_{sep}$  is the distance of separation between the two manipulators. For roll case,  $d_{sep}$  is  $l_a + l_p$  and for pitch case,  $d_{sep}$  is  $l_r + l_p$ .

## 5. Experiments

Experiments were carried out to observe the UAV take-off from sloped surfaces. The UAV is placed on a sloped rigid surface and controlled to take-off. In the first trial, as soon as the UAV's propellers spun up, the UAV slid down the slope, fell off and crashed as shown in Figure 8. The sliding occurred because the spinning propellers created a small thrust, which reduced the friction of the UAV's ground contact. Another trial was performed similar to the first case. This time as soon as the UAV started sliding when the propellers spun up, the thrust increased to avoid sliding by the remote operator, to take

off from the surface quickly. However, since the UAV attitude was not leveled, this trial resulted in crashing into a close-by wall as shown in Figure 9.



**Figure 8.** Conventional UAV take-off from a sloped surface resulting in sliding and falling down.



**Figure 9.** Conventional UAV take-off from a sloped surface resulting in sliding and crashing into a wall.

We performed experiments to test the adaptive leveling system designed in this work using a three-manipulator system. The manipulator system is designed to carry out heterogeneous tasks with high efficiency. Various experiments using a three-arm aerial manipulator system for landing, grasping and obstacle avoidance were discussed in our previous work [12]. In this work, we only discuss the experiment on maintaining stable posture of the airframe landed on an unstable surface.

To perform the experiment, we setup a platform with a large rigid sheet horizontally on top of a small half-spherical base at its center such that its slope can be manually tilted in its centered roll and pitch axes. By default, the rigid sheet stays sloped at an angle such that one of its sides touches the ground under it. The UAV is then manually controlled by a remote operator to adaptive land on the platform, using the same approach of our work in [13]. After landing, the rotors are shut off completely to make sure the UAV is standing on its own with its weight distributed between the three manipulators. After the UAV is landed and is stable, the platform is moved manually by an assisting person in both its roll and pitch axes. The change in the slope of the platform disturbs the stable posture of the airframe, therefore tends to change its angle accordingly.

An experiment was performed without the adaptive posture control. The resulting graph plotted for roll and pitch angle of the airframe is shown in Figure 10. The angle of the airframe changes with the change in the slope of the platform, because of the fixed posture of the manipulators. Without adaptive posture control, it was often not possible to take off from a sloped angle of the airframe since the flight controller indicated an erroneous take-off position in most of the cases. Of the cases where the UAV was able to take off, the take-off was not perfectly vertical from the ground and may therefore crash into wall or other objects if a wide empty space around UAV is unavailable.

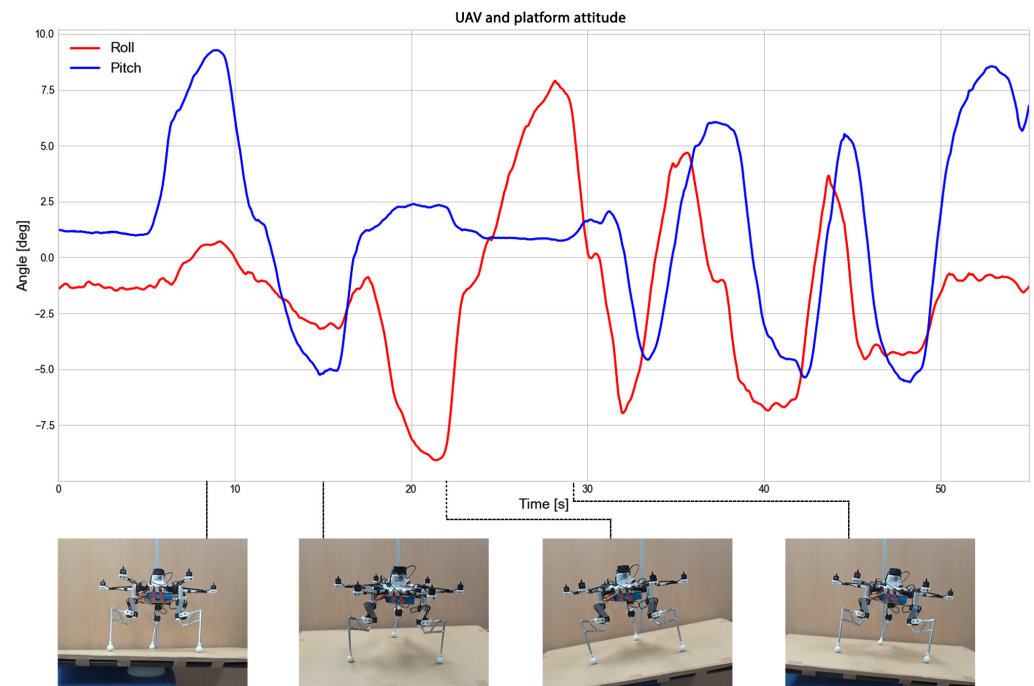


**Figure 10.** Roll and pitch angles of the UAV and platform attitude during the experiment without leveling control against surface slope change.

The same experiment was repeated with the adaptive posture control. By checking the direction of the load from torque sensors in the joint motors of the last link, it can ensure if that manipulator is touching a surface or not. The adaptive control is activated when all the manipulators are touching to a surface. By activating the adaptive posture control, the manipulators adjust itself using the flight controllers IMU sensor data feedback to keep the airframe in a stable posture parallel to the earth's horizon. This results in the UAV being able to take off at any instant, even during rapid change of the landing surface angle during take off. The resulting experimental data for roll and pitch angle of the UAV is seen in the graph in Figure 11. Even though the surface shifts to about  $10^\circ$  (a 17.6% incline), the UAV is seen to be able to adjust within  $2^\circ$  error. The time required to horizontally level the UAV platform with the adaptive landing gear starting from a 17.6% incline, takes less than 1 s. This means the landing gear movement is fast enough to counter quick continuous changes in landing surface angle as seen in Figure 10. The UAV is then made to take off from the platform at a random sloped angle. It was successfully able to take off since the airframe is always parallel to the horizon. After take-off, the roll and pitch angles visible in the graph change rapidly due to vibration and attitude changes during the UAV flight.

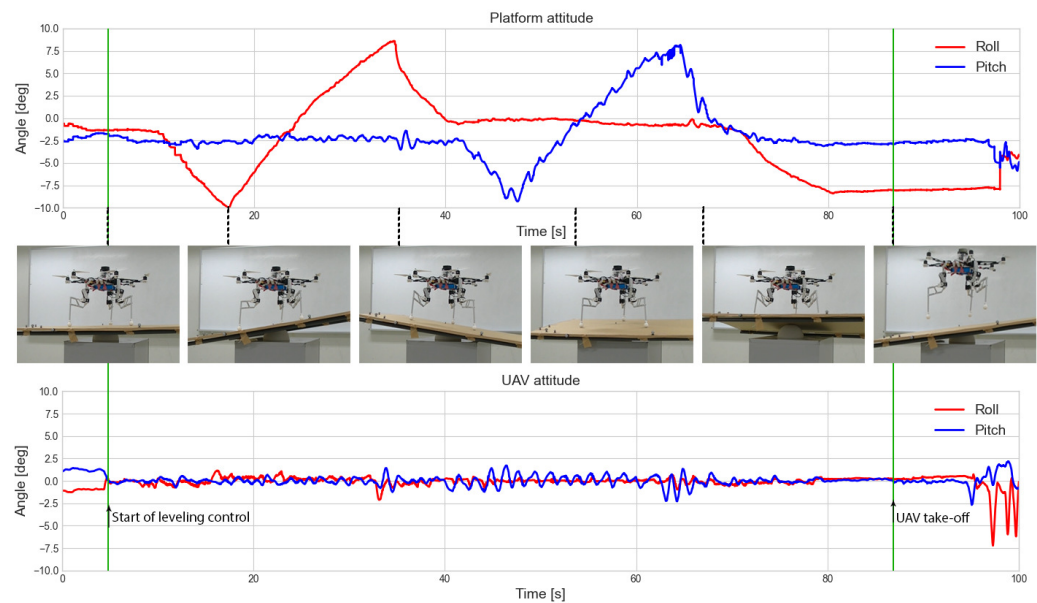


**Figure 11.** Roll and pitch angles of the UAV and platform attitude during the experiment to maintain the airframe horizontal against surface slope change.

## 6. Discussion

The conducted experiments of a conventional landing gear UAV take-off from a sloped surface show that the UAV cannot safely move vertically upwards when taking-off from a sloped surface. In the case of UAV take-off from a flat surface, the thrust vector generated by the propellers of the UAV points downwards and therefore lifts the UAV upwards. From the conventional UAV take-off experiments from sloped surface shown in Figures 8 and 9, it is observed that the UAV posture remains tilted even after take-off. Therefore, the direction of the thrust vector is not pointing downwards, resulting in a push in non-perpendicular direction to the horizon, making the UAV move diagonally. Therefore, the UAV requires a wider open space to level itself after take-off in a tilted attitude or the UAV may crash into structures on its flightpath. The videos of all the experiments can be found in the Supplementary Material.

The designed manipulator system uses a custom parallel link mechanism and therefore requires only one actuator to change the height of the manipulator while keeping the tip perpendicular to the horizon. From conducted experiments we show that it is possible to stand and stabilize the airframe, using three manipulators to maintain the airframe parallel to the horizon against the change in the surface angle. The IMU sensor data from the UAV's flight controller was used to obtain the UAV's roll and pitch angle. Depending on the roll and pitch angle change, the three manipulators height is controlled accordingly to maintain the airframe parallel to the horizon. Proper PD parameter tuning is required to quickly respond with the manipulators to the smallest change in the airframe angle, to keep the UAV stable. There is, however, a limit to the maximum angle change that can be compensated by the manipulator system and this limit depends on the physical design of the manipulator. The maximum angle change after which the UAV encounters a roll over event is calculated using Equations (8)–(11), which are all dependent on manipulator placement  $l_n$ . The maximum roll and pitch angles of a surface till which the manipulator system can maintain the airframe horizontal is  $35.29[^\circ]$  and  $39.29[^\circ]$  respectively (a 70.78% or 81.82% slope), obtained using (15). In addition, a sudden large change in the airframe angle can disturb the UAV's stability and can lead to rollover before the manipulators starts stabilizing the angle.

Although we show that is possible to realize the airframe stabilization with a minimum of three manipulators, more than three can provide better stability, at the cost of shorter flight time. The tips of the manipulator are made rounded with silicon outer layer, which

provide some amount of friction in slopes but when landing on sloped surfaces with a lot less friction than the surfaces used in the experiments of this work, a material with higher friction is necessary at the tips of the manipulators.

## 7. Conclusions

In this work, we describe the design and development of a novel three-arm manipulator system for a UAV using a custom build parallel link mechanism, novel to aerial manipulation. The system is designed so that it can be used to carry out various heterogeneous tasks with the same set of manipulators. The manipulators are made light-weight and require less actuation force for the tasks realized in our previous work [12]. Furthermore, the controlling of the manipulator system to maintain the airframe parallel to the horizon when landed on an unstable surface with changing elevations is described and shown in experiments. In experiments we show that the UAV can safely take-off from a sloped, unstable or rocking surface. A UAV system such as this is suitable to be deployed in an unfamiliar or disaster struck sites, due to its ability to land in uneven or shifting ground without losing its ability to take off again, as a UAV with traditional landing gear would.

**Supplementary Materials:** The following are available at <https://www.mdpi.com/article/10.3390/app11199157/s1>, Video S1: Supporting Video.mp4.

**Author Contributions:** Contributions of the authors are as follows. H.P.: designed and developed the proposed system, performed experiments, analyzed the data, writing—original draft preparation, writing—review and editing; R.M. and T.K.: advice on the system design, performed experiments, writing—review and editing; R.L.: development of idea, advice on the system design and experiments, writing—review and editing; K.S.: supervision, advice on the system design and experiments, writing—review and editing. All authors have read and agreed to the published version of the manuscript.

**Funding:** This research received no external funding.

**Conflicts of Interest:** The authors declare no conflict of interest.

## Abbreviations

The following abbreviations are used in this manuscript:

UAV	Unmanned aerial vehicle
VTOL	Vertical take-off and landing
DOF	Degree of freedom
IMU	Inertial measurement unit
PLA	Polylactic acid
COG	Center of gravity

## References

1. Recchiuto, C.T.; Sgorbissa, A. Post-disaster assessment with unmanned aerial vehicles: A survey on practical implementations and research approaches. *J. Field Robot.* **2018**, *35*, 459–490. [[CrossRef](#)]
2. Ezequiel, C.A.F.; Cua, M.; Libatique, N.C.; Tangonan, G.L.; Alampay, R.; Labuguen, R.T.; Favila, C.M.; Honrado, J.L.E.; Canos, V.; Devaney, C.; et al. UAV aerial imaging applications for post-disaster assessment, environmental management and infrastructure development. In Proceedings of the 2014 International Conference on Unmanned Aircraft Systems (ICUAS), Orlando, FL, USA, 27–30 May 2014; pp. 274–283.
3. Korpela, C.; Orsag, M.; Oh, P. Towards valve turning using a dual-arm aerial manipulator. In Proceedings of the 2014 IEEE/RSJ International Conference on Intelligent Robots and Systems, Chicago, IL, USA, 14–18 September 2014; pp. 3411–3416.
4. Papachristos, C.; Alexis, K.; Tzes, A. Efficient force exertion for aerial robotic manipulation: Exploiting the thrust-vectoring authority of a tri-tiltrotor uav. In Proceedings of the 2014 IEEE international conference on robotics and automation (ICRA), Hong Kong, China, 31 May–7 June 2014; pp. 4500–4505.
5. Lin, T.J.; Long, S.; Stol, K.A. Automated perching of a multirotor UAV atop round timber posts. In Proceedings of the 2018 IEEE/ASME International Conference on Advanced Intelligent Mechatronics (AIM), Auckland, New Zealand, 9–12 July 2018; pp. 486–491.

6. Pope, M.T.; Cutkosky, M.R. Thrust-assisted perching and climbing for a bioinspired UAV. In *Conference on Biomimetic and Biohybrid Systems*; Springer: Berlin/Heidelberg, Germany, 2016; pp. 288–296.
7. Paul, H.; Ono, K.; Ladig, R.; Shimonomura, K. A multirotor platform employing a three-axis vertical articulated robotic arm for aerial manipulation tasks. In *Proceedings of the 2018 IEEE/ASME International Conference on Advanced Intelligent Mechatronics (AIM)*, Auckland, New Zealand, 9–12 July 2018; pp. 478–485.
8. Koparan, C.; Koc, A.B.; Privette, C.V.; Sawyer, C.B.; Sharp, J.L. Evaluation of a UAV-assisted autonomous water sampling. *Water* **2018**, *10*, 655. [[CrossRef](#)]
9. Araar, O.; Aouf, N.; Vitanov, I. Vision based autonomous landing of multirotor UAV on moving platform. *J. Intell. Robot. Syst.* **2017**, *85*, 369–384. [[CrossRef](#)]
10. Rodriguez-Ramos, A.; Sampedro, C.; Bavlé, H.; De La Puente, P.; Campoy, P. A deep reinforcement learning strategy for UAV autonomous landing on a moving platform. *J. Intell. Robot. Syst.* **2019**, *93*, 351–366. [[CrossRef](#)]
11. Manivannan, V.; Langley, J.P.; Costello, M.; Ruzzene, M. Rotorcraft slope landings with articulated landing gear. In *Proceedings of the AIAA Atmospheric Flight Mechanics (AFM) Conference*, Boston, MA, USA, 19–22 August 2013; p. 5160.
12. Paul, H.; Miyazaki, R.; Ladig, R.; Shimonomura, K. TAMS: Development of a multipurpose three-arm aerial manipulator system. *Adv. Robot.* **2021**, *35*, 31–47. [[CrossRef](#)]
13. Paul, H.; Miyazaki, R.; Ladig, R.; Shimonomura, K. Landing of a multirotor aerial vehicle on an uneven surface using multiple on-board manipulators. In *Proceedings of the 2019 IEEE/RSJ International Conference on Intelligent Robots and Systems (IROS)*, Macau, China, 3–8 November 2019; pp. 1926–1933.
14. Ikeda, T.; Yasui, S.; Minamiyama, S.; Ohara, K.; Ashizawa, S.; Ichikawa, A.; Okino, A.; Oomichi, T.; Fukuda, T. Stable impact and contact force control by UAV for inspection of floor slab of bridge. *Adv. Robot.* **2018**, *32*, 1061–1076. [[CrossRef](#)]
15. Rönna, A.; Heppner, G.; Nowicki, M.; Dillmann, R. LAURON V: A versatile six-legged walking robot with advanced maneuverability. In *Proceedings of the 2014 IEEE/ASME International Conference on Advanced Intelligent Mechatronics*, Besacon, France, 8–11 July 2014; pp. 82–87.
16. Qin, L.; Liang, X.; Huang, H.; Chui, C.K.; Yeow, R.C.H.; Zhu, J. A versatile soft crawling robot with rapid locomotion. *Soft Robot.* **2019**, *6*, 455–467. [[CrossRef](#)] [[PubMed](#)]
17. Bandyopadhyay, T.; Steindl, R.; Talbot, F.; Kottege, N.; Dungavell, R.; Wood, B.; Barker, J.; Hoehn, K.; Elfes, A. Magneto: A versatile multi-limbed inspection robot. In *Proceedings of the 2018 IEEE/RSJ International Conference on Intelligent Robots and Systems (IROS)*, Madrid, Spain, 1–5 October 2018; pp. 2253–2260.
18. Multi-Tasking Robots—Doing the Dangerous Work, so Humans Don't Have to. Available online: <https://stfc.ukri.org/news-events-and-publications/features/multi-tasking-robots/> (accessed on 11 June 2021).
19. Motlagh, N.H.; Bagaa, M.; Taleb, T. UAV-based IoT platform: A crowd surveillance use case. *IEEE Commun. Mag.* **2017**, *55*, 128–134. [[CrossRef](#)]
20. Mathew, N.; Smith, S.L.; Waslander, S.L. Planning paths for package delivery in heterogeneous multirobot teams. *IEEE Trans. Autom. Sci. Eng.* **2015**, *12*, 1298–1308. [[CrossRef](#)]
21. Doherty, P.; Rudol, P. A UAV search and rescue scenario with human body detection and geolocalization. In *Australasian Joint Conference on Artificial Intelligence*; Springer: Berlin/Heidelberg, Germany, 2007; pp. 1–13.
22. Olsson, P.M.; Kvarnström, J.; Doherty, P.; Burdakov, O.; Holmberg, K. Generating UAV communication networks for monitoring and surveillance. In *Proceedings of the 2010 11th International Conference on Control Automation Robotics & Vision*, Singapore, 7–10 December 2010; pp. 1070–1077.
23. Malandrino, F.; Rottondi, C.; Chiasserini, C.F.; Bianco, A.; Stavrakakis, I. Multiservice UAVs for Emergency Tasks in Post-disaster Scenarios. In *Proceedings of the ACM MobiHoc Workshop on Innovative Aerial Communication Solutions for First Responders Network in Emergency Scenarios*, Catania, Italy, 2 July 2019; pp. 18–23.
24. Puttock, A.; Cunliffe, A.; Anderson, K.; Brazier, R.E. Aerial photography collected with a multirotor drone reveals impact of Eurasian beaver reintroduction on ecosystem structure. *J. Unmanned Veh. Syst.* **2015**, *3*, 123–130. [[CrossRef](#)]
25. Ruggiero, F.; Lippiello, V.; Ollero, A. Aerial manipulation: A literature review. *IEEE Robot. Autom. Lett.* **2018**, *3*, 1957–1964. [[CrossRef](#)]
26. Alaimo, A.; Artale, V.; Milazzo, C.; Ricciardello, A.; Trefiletti, L. Mathematical modeling and control of a hexacopter. In *Proceedings of the 2013 International Conference on Unmanned Aircraft Systems (ICUAS)*, Atlanta, GA, USA, 28–31 May 2013; pp. 1043–1050.
27. Pose, C.D.; Giribet, J.I.; Ghersin, A.S. Hexacopter fault tolerant actuator allocation analysis for optimal thrust. In *Proceedings of the 2017 International Conference on Unmanned Aircraft Systems (ICUAS)*, Miami, FL, USA, 13–16 June 2017; pp. 663–671.
28. Baskaya, E.; Hamandi, M.; Bronz, M.; Franchi, A. A Novel Robust Hexarotor Capable of Static Hovering in Presence of Propeller Failure. *IEEE Robot. Autom. Lett.* **2021**, *6*, 4001–4008.
29. Mazeh, H.; Saied, M.; Shraim, H.; Francis, C. Fault-tolerant control of an hexarotor unmanned aerial vehicle applying outdoor tests and experiments. *IFAC-PapersOnLine* **2018**, *51*, 312–317. [[CrossRef](#)]
30. Suarez, A.; Jimenez-Cano, A.E.; Vega, V.M.; Heredia, G.; Rodriguez-Castaño, A.; Ollero, A. Design of a lightweight dual arm system for aerial manipulation. *Mechatronics* **2018**, *50*, 30–44. [[CrossRef](#)]
31. Kim, S.; Seo, H.; Choi, S.; Kim, H.J. Vision-guided aerial manipulation using a multirotor with a robotic arm. *IEEE/ASME Trans. Mechatronics* **2016**, *21*, 1912–1923. [[CrossRef](#)]

32. Molina, J.; Hirai, S. Pruning tree-branches close to electrical power lines using a skew-gripper and a multirotor helicopter. In Proceedings of the 2017 IEEE International Conference on Advanced Intelligent Mechatronics (AIM), Munich, Germany, 3–7 July 2017; pp. 1123–1128.
33. Rashad, R.; Engelen, J.B.; Stramigioli, S. Energy tank-based wrench/impedance control of a fully-actuated hexarotor: A geometric port-hamiltonian approach. In Proceedings of the 2019 International Conference on Robotics and Automation (ICRA), Montreal, QC, Canada, 20–24 May 2019; pp. 6418–6424.
34. Ladig, R.; Paul, H.; Miyazaki, R.; Shimonomura, K. Aerial Manipulation Using Multirotor UAV: A Review from the Aspect of Operating Space and Force. *J. Robot. Mechatronics* **2021**, *33*, 196–204. [[CrossRef](#)]
35. Ollero, A.; Tognon, M.; Suarez, A.; Lee, D.; Franchi, A. Past, Present, and Future of Aerial Robotic Manipulators. *IEEE Trans. Robot.* **2021**, 1–20. [[CrossRef](#)]